View metadata, citation and similar papers at core.ac.uk

brought to you by CORE

provided by Harvard University - DASH

DIGITAL ACCESS TO SCHOLARSHIP AT HARVARD

High Spatial Resolution Kelvin Probe Force Microscopy With Coaxial Probes

The Harvard community has made this article openly available. Please share how this access benefits you. Your story matters.

Citation	Brown, Keith A., Kevin J. Satziner, and Robert M. Westervelt. 2012. High spatial resolution Kelvin probe force microscopy with coaxial probes. Nanotechnology 23(11): 115703.
Published Version	doi:10.1088/0957-4484/23/11/115703
Accessed	February 19, 2015 10:28:53 AM EST
Citable Link	http://nrs.harvard.edu/urn-3:HUL.InstRepos:9639955
Terms of Use	This article was downloaded from Harvard University's DASH repository, and is made available under the terms and conditions applicable to Open Access Policy Articles, as set forth at http://nrs.harvard.edu/urn-3:HUL.InstRepos:dash.current.terms-of-use#OAP

(Article begins on next page)

High spatial resolution Kelvin probe force microscopy with coaxial probes

Keith A Brown,[1,*] Kevin J Satzinger,[2] and Robert M Westervelt[1,3]

[1]School of Engineering and Applied Sciences, Harvard University, Cambridge, MA 02138, USA

[2]Department of Physics, Truman State University, Kirksville, MO 63501, USA

[3]Department of Physics, Harvard University, Cambridge, MA 02138, USA

E-mail: westervelt@seas.harvard.edu

Abstract

Kelvin probe force microscopy (KPFM) is a widely used technique to measure the local contact potential difference (CPD) between an AFM probe and the sample surface *via* the electrostatic force. The spatial resolution of KPFM is intrinsically limited by the long range of the electrostatic interaction, which includes contributions from the macroscopic cantilever and the conical tip. Here, we present coaxial AFM probes in which the cantilever and cone are shielded by a conducting shell, confining the tip-sample electrostatic interaction to a small region near the end of the tip. We have developed a technique to measure the true CPD despite the presence of the shell electrode. We find the behavior of these probes agrees with an electrostatic model of the force, and we observe a factor of 5 improvement in spatial resolution relative to unshielded probes. Our discussion centers on KPFM, but the field confinement offered by these probes may improve any variant of electrostatic force microscopy.

PACS numbers: 07.79.Lh and 73.30.+y

[*] Currently at Northwestern University

1. Introduction

Kelvin probe force microscopy (KPFM) is a widely used technique to measure the contact potential difference (CPD) between an atomic force microscope (AFM) probe and a surface [1]. KPFM has seen extensive use characterizing semiconductors [2, 3], oxide material properties [4, 5], photovoltaic devices [6], and biomolecules [7, 8]. KPFM is intrinsically limited by the long range of the electrostatic interaction [9, 1]. The result of long-range contributions is that the electrostatic contribution from the region just below the tip is a small part of the entire interaction [10], and extreme care must be taken to remove topographic artifacts [11, 12]. Despite these limitations, atomic resolution has been achieved by operating in high vacuum to make the instrument sensitive enough to detect vibration amplitude with precision ~ 10^{-4} nm and frequency shifts at ~ 5 parts in 10^7 [13, 14, 15]. In addition, specialized probes have been developed to improve the resolution of KPFM operating in ambient conditions, such as probes with carbon nanotubes adhered to their tip [16] and cantilevers with their higher mechanical resonance modes engineered to minimally impact KPFM measurements [17].

Coaxial AFM probes can improve KPFM by confining the electric field to a small region at the tip of the AFM probe. Figure 1(a) illustrates the need for field confinement with an axisymmetric electrostatic simulation (Maxwell 2D — Ansys Inc.) in which an unshielded conducting tip is held at 1 V near a grounded substrate. The electrostatic potential ϕ varies in the whole region, denoting widespread high electric field. In contrast, figure 1(b) shows ϕ simulated near the tip of a coaxial probe where the core conductor is held at 1 V and the shell and substrate are grounded. The field is confined to the region at the tip of the probe. The improvement in confinement is evident in figure 1(c) in which the electric fields 50 nm below the coaxial and unshielded probes are plotted as the black and red lines respectively. Both curves are peaked directly below the probe but the field from the coaxial probe falls off much more quickly and does not exhibit the long range shoulders visible for the unshielded probe. The improvement in field confinement makes coaxial probes capable of improving the spatial resolution of any electrostatic force microscopy technique. Previously, coaxial probes have been used for scanning near field microwave microscopy [18], scanning conductance microscopy [19], and imaging with dielectrophoresis [20].

In this paper, we demonstrate enhanced spatial resolution KPFM with coaxial probes, such as the probe shown in figure 2. We begin by describing how KPFM is modified with the addition of a shell electrode and present a method to measure the true CPD despite the complication of the shell electrode. The experimental apparatus and technique used to fabricate coaxial probes are then described. Coaxial probes are calibrated to remove the effect of the shell and we find the behavior of the probes to be in agreement with our electrostatic model of coaxial probes. Finally, we demonstrate KPFM imaging with

coaxial probes and demonstrate a factor of 5 improvement in spatial resolution relative to an unshielded probe.

2. KPFM with coaxial probes

KPFM provides a measurement of the contact potential difference (CPD) v_{12} between a conducting AFM probe and a sample [1]. The tip and sample are capacitively coupled with capacitance C_{12}, and a voltage $V_1 = V_{DC} + V_{AC} \sin(2\pi ft)$ is applied to the probe while the sample is grounded, with potential $V_2 = 0$. The application of V_1 leads to an electrostatic force F that acts to reduce the tip-sample separation z. The force has a component oscillating at frequency f whose magnitude is given by:

$$F_f = \frac{\partial C_{12}}{\partial z} V_{AC} \left(V_{DC} - v_{12} \right) \tag{1}$$

By setting f to the cantilever's principle vibrational resonance frequency f_0, the force F_f drives the vibrational resonance mode of the cantilever. The vibration amplitude A may be nulled by adjusting V_{DC} with feedback. The value of V_{DC} when A is minimized is defined as the Kelvin voltage V_K, and we see that $V_K = v_{12}$ for a uniform sample, providing a measure of the tip-sample CPD.

The addition of a coaxial shell electrode complicates the electrostatic picture of KPFM, as shown in figure 3(a). There is now a tip-shell capacitance C_{13} and a shell-sample capacitance C_{23} in addition to the tip-sample capacitance C_{12}. The introduction of these capacitances is similar to the "stray capacitance problem" in the scanning Kelvin probe literature, a non-AFM based technique to measure CPD [21, 22, 23]. Figure 3(c) shows the capacitances in this system calculated by finite element simulation (Maxwell 2D — ANSYS Inc.) using the axisymmetric region shown in figure 3(b). The largest capacitance is C_{13}.

Care must be taken to remove the electrostatic effect of the conducting shell to perform KPFM with a coaxial probe. The electrostatic force is proportional to the derivative of capacitances with respect to tip-sample distance z, so we define $C'_{ij} \equiv \frac{\partial C_{ij}}{\partial z}$. Figure 3(d) shows C'_{ij} *vs.* z calculated by the finite difference method from the capacitance data in figure 3(c). While C'_{23} has the largest magnitude, so long as there is no AC voltage on the shell electrode or the substrate, it will only contribute to the DC deflection. At practical separations ($z \sim 50$ nm), C'_{12} and C'_{13} have similar magnitudes, so the effect of C'_{13} must be removed to make a true measurement of the tip-sample CPD.

By adjusting the control voltages in KPFM, it is possible to perform KPFM with a coaxial probe and still attain an accurate measurement of the tip-sample CPD. We apply voltages $V_1 = V_{AC} \sin(2\pi ft)$ to

the probe, $V_2 = V_{DC}$ to the sample, and $V_3 = V_S$ to the shell. Since an AC voltage is only applied to the tip, only terms with C'_{12} or C'_{13} will appear in F_f. We can again adjust V_{DC} to set $A = 0$ and we find the Kelvin voltage:

$$V_K = -\nu_{12} - \frac{C'_{13}}{C'_{12}}\left(V_S + \nu_{13}\right), \tag{2}$$

where ν_{13} is the tip-shell CPD. The second term is the contribution from the shell electrode, which can include topographic artifacts, because C'_{13}/C'_{12} depends on z, as seen in figure 3(d). As demonstrated below, it is possible to measure the contact potential difference ν_{12} without the influence of the shell, by zeroing the second term by setting the shell voltage to $V_S = -\nu_{13}$.

3. Experimental

Coaxial AFM probes such as the one shown in figure 2 are fabricated by a technique similar to previously reported methods [24, 20, 25]. Briefly, conducting AFM probes (Arrow-NCPt — NanoWorld AG) are coated with 25 nm of Ti as an adhesive layer by electron-beam evaporation (EE). An insulator is then formed by 50 nm of low stress silicon nitride deposited *via* plasma-enhanced chemical vapor deposition (PECVD). An additional ~ 2 μm thick insulating bilayer of silicon dioxide and silicon nitride is deposited with PECVD on the cantilever holder to mechanically and electrically reinforce it. Finally, a 30 nm/50 nm bilayer of Ti/Au is deposited *via* EE to form the shell electrode. The coaxial electrodes are exposed by a focused ion beam etch.

Reference samples for Kelvin probe measurements are fabricated by standard nanofabrication techniques. Chips of highly n-doped polished Si wafers (Silicon Quest International, Inc.) are diced and chemically cleaned. Large (~ mm^2) rectangular regions are patterned with photoresist (S1813 — Shipley) using photolithography and metals are deposited with EE. Two samples are used for KPFM in this study, bare Si wafers with 20 nm thick Cr regions and Au-coated wafers with regions consisting of a 25 nm Pt layer with a 5 nm Ti sticking layer.

KPFM is performed using a two-pass technique with a commercial AFM (MFP-3D — Asylum Research) with additional circuitry shown in figure 4. In the first pass, the AFM is driven mechanically and the topography is imaged by amplitude-modulation AFM. In alternating passes, the probe retraces the previously captured topographic profile and the probe is driven electrically. The feedback loop shown in figure 4 adjusts V_{DC} to a value that zeroes the vibrational amplitude A. The value of V_{DC} that minimizes A is recorded as V_K. These interlaced scans are repeated to generate an image. The AFM is typically scanned at 5 μm/s and the KPFM retrace is at done at the same tip-sample separation z as the topographic scan. All images of V_K have the mean of each trace subtracted to reduce the effect of drift during the scan.

For all KPFM data shown, we use the same imaging parameters which are chosen to be typical for AM-KPFM done in ambient conditions. We scan a 90 μm by 22.5 μm region in 128 lines while recording 4096 points per line. The integral gain is set to 10 and no proportional gain. The amplitude sensitivity of each cantilever is tuned with a force-distance curve so as to set the free-space amplitude to 83 nm and the set-point amplitude to 50 nm. During the second pass there is no z-offset so the tip retraces a path 50 nm over the substrate. During these interleaved passes, the Kelvin voltage is maintained with an integral gain of 4, no proportional gain, and an AC-voltage with amplitude of 3 V. The typical resonance frequency of an Arrow-NCPt cantilever is found to be near 260 kHz.

In order to correctly generate the control voltages for coaxial KPFM, additional voltage sources, shown in figure 4, are added to the commercial AFM. The Asylum Research Controller (ARC) generates V_{AC} and V_{DC}, and controls the feedback loop by measuring A with optical readout of the cantilever deflection. We separate V_{AC} and V_{DC} with high pass and low pass filters. The AC voltage V_{AC} is separated by a single pole high pass RC filter with a corner frequency at 34 kHz, which passes 99% of V_{AC} to V_1. The DC voltage V_{DC} is separated by a 5 pole low pass LR filter with a corner frequency at 25 kHz, which attenuates V_{AC} by ~ -80 dB and allows V_{DC} to reach V_3. The bias voltage V_S is generated by an external voltage source (Agilent 33220A) which is in parallel with a 10 μF shunt capacitor to provide a low impedance path to ground for RF voltages. Electrical contacts to the coaxial AFM probe are provided by a custom tip holder with separate electrical contacts to the top and bottom of the probe.

4. Results

Before using a coaxial Kelvin probe to measure the contact potential difference (CPD), it is necessary to remove unwanted shifts in the Kelvin voltage V_K caused by the shell. From equation (2), one can see that these shifts can be removed by adjusting the shell voltage to the value $V_S = -v_{13}$ where v_{13} is the contact potential difference between the coaxial core and the shell. Experimentally, one can calibrate the tip voltage at this value by finding the shell voltage $V_S = V_S^c$ at which the measured Kelvin voltage V_K is independent of the tip-sample separation z.

Figure 5 demonstrates the calibration procedure using Kelvin probe data recorded by a coaxial probe scanned above a uniform gold film. Figure 5(a) shows the mean Kelvin voltage V_K over a 10x10 μm^2 scan at a height z = 100 nm. The Kelvin voltage V_K increases linearly with shell voltage V_S, as predicted by equation (2); the standard deviation in V_K is smaller than the size of the points. Figure 5(b) shows how V_S can be calibrated by measuring ΔV_K vs. V_S at three values of z. Here $\Delta V_K = V_K - V_{K100}$ where V_{K100} = (5.0 x V_S) - 481 mV is the linear fit to the data at z = 100 nm shown in figure 4(a). The data for ΔV_K vs. V_S for three straight lines with different slopes, and they intersect at the same shell

voltage V_S^c = 1184 ± 1 mV. When $V_S = V_S^c$, the second term in equation (2) is zero, and the effect of the shell electrode is removed.

The measured slopes of V_K *vs.* V_S agree with our electrostatic model of coaxial probes: equation (2) predicts $\partial V_K / \partial V_S = C'_{13}/C'_{12}$. Figure 4(c) shows measurements of C'_{13}/C'_{12} taken from the slope of the measured Kelvin voltage V_K *vs.* the shell voltage V_S for five coaxial probes. To compare these measurements with theory, we use our simulations for C'_{13} and C'_{12} from figure 3(d). We include a constant contribution to C'_{13} from deformation of the cantilever capacitor [26], which for identically prepared probes is ~ 0.1 aF/nm. The simulated cantilever-sample interaction is C'_{12} ~ 0.03 aF/nm, roughly an order of magnitude smaller than an unshielded cantilever. The simulated ratio C'_{13}/C'_{12} shown by the line in figure 4(c), is in good agreement with our observations.

Figure 6 compares KPFM images obtained with a coaxial probe and an unshielded conducting probe. The coaxial probe sharpens the images and eliminates artifacts by confining the electric field to a small region near the end of the probe. Figure 6(a) shows a KFPM image taken with an unshielded probe of a flat sample where the left region is gold and the right region is platinum. The measured Kelvin voltage V_K continues to change tens of microns to the right of the step, due the long range electrostatic interaction of the cantilever with the sample. Figure 6(b) shows a KPFM image of the same sample with a coaxial probe; it exhibits a sharper transition between materials with no long range contributions. The shell electrode sufficiently shields the cantilever so its contribution is small compared to the coaxial electrodes at the tip. The improvement in the step fidelity is apparent in figure 6(c), which shows the average line trace across the transition between materials for each method.

A properly tuned coaxial KPFM measurement removes topographic artifacts common in measurements of V_K. Figure 6(d) and 6(e) show KPFM images taken with an unshielded and coaxial probe respectively of different regions of a sample with heavily doped silicon in the left region and chrome in the right region. The image taken with the coaxial probe appears smoother, which can be seen more clearly in figure 6(f) which depicts the normalized average of all 128 line traces. The red line corresponds to the unshielded probe and topographic artifacts are visible near the interface. The black line shows the data collected with the coaxial probe. It is smooth and without topographic artifacts as the calibration procedure makes this measurement technique insensitive to variation in z.

Coaxial probes demonstrate a factor of 5 improvement in spatial resolution compared with unshielded KPFM probes. The spatial resolution is estimated as the minimum distance x_{step} required for V_K to transition by 50% of the full value of the step from one material to another. The asymmetry of the curves makes the minimum distance necessary to change 50% of the curve a relevant measure. For

unshielded probes, we find x_{step} = 1.6 μm from figure 6(c) and x_{step} = 1.7 μm from figure 6(f). Coaxial probes offer a large improvement, giving x_{step} = 410 nm from figure 6(c) and x_{step} = 280 nm from figure 6(f), commensurate with the diameters of the coaxial probes used in each measurement.

5. Discussion

Simulations of the electric field profile produced by unshielded and coaxial probes above a conducting substrate are shown in figures 7(a) and 7(b) for a range of tip-sample separations z. These simulations show that the spatial resolution of coaxial probes is determined by the tip geometry, and demonstrate how a coaxial probe can be resistant to topographical artifacts. For the unshielded probe (figure 7(a)), the electric field distribution narrows considerably as z is decreased from 50 nm to 10 nm. Decreasing z improves the spatial resolution, but this also means that variations in z will strongly affect the point-spread function of the measurement, leading to topographical artifacts. In addition, broad shoulders to the electric field profile still exist when the height z is equal to the tip radius of 10 nm, adding long-range contributions to any electrostatic measurement. For the coaxial probe (Fig. 7(b)), decreasing z causes the electric field profile to adopt a nearly trapezoidal shape with a width that is simply the diameter of the core conductor. Away from the core, the field rapidly decays toward zero across the insulator thickness. The relative insensitivity of the field profile to z makes this technique resistant to topographical artifacts.

We have demonstrated that coaxial AFM probes can perform Kelvin probe force microscopy with enhanced spatial resolution. A theoretical model for performing KPFM with a coaxial tip to measure the tip-sample contact potential difference has been developed. Coaxial AFM probes with 50 nm electrode spacing at the tip were fabricated and tested with a commercial AFM. Unwanted shifts in the Kelvin voltage by the shell electrode can be avoided by calibrating the shell bias voltage V_S to give the same Kelvin voltage V_K at different tip-sample separations z. We find that coaxial probes have the following advantages: they reduce capacitive coupling between the cantilever and the sample, decrease topographical artifacts, and improve the spatial width of a transition from one material to another, from ~ 1.6 μm to ~ 300 nm in our experiments. The spatial resolution of a coaxial tip can be improved by creating tips with thinner insulating layers and finer centre conductors. The dielectric breakdown strength of SiNx films is ~ 0.5 V/nm,[27] so insulators as thin as 10 nm would be sufficient to withstand typical voltages in an KPFM measurement. One method for creating centre conductors of nearly atomic sharpness would be to polish the multilayer tip on an abrasive conducting surface during fabrication until electrical contact is made between the centre conductor and the surface. The blunt shape of these tips could be a disadvantage for topographical imaging, although for the relatively flat samples studied here,

we did not notice any degradation in topographic image quality. In order to preserve tip sharpness for topographical imaging, one could mill the tip at an angle or use a chemical etch to create retain a protruding centre conductor.

Coaxial probes improve the spatial resolution by confining the electric field to a region near the end of the tip which means that coaxial probes promise to improve the quality of any imaging technique that is based on the electrostatic interaction. It is important to reiterate that this is a demonstration of the improved performance of a coaxial probe over a standard probe rather than an attempt to surpass state of the art resolution in KPFM measurements. The mm-scale resolution resulting from the imaging parameters and unshielded probe used in this work are not uncommon for ambient AM-KPFM measurements.[28] Lower drive amplitudes or decreased tip-sample separations are also commonly used and provide greatly improved resolution.[29] As discussed in the introduction, many techniques exist for performing KPFM with enhanced resolution[13, 14, 15] including reducing the tip-sample separation,[28] operating in vacuum,[30] and using frequency modulation (FM) rather than amplitude modulation.[28,30] Coaxial probes may be used in vacuum and are compatible with FM-KPFM so in principle they could be used to improve the spatial resolution in these modalities. As a further potential improvement, it is possible to employ a one-pass technique where the surface potential and topography are measured simultaneously.[14]

Acknowledgements

We acknowledge support by the Department of Defense through a National Defense Science & Engineering Graduate (NDSEG) Fellowship, the National Nanotechnology Infrastructure Network through the Research Experience for Undergraduates Program through National Science Foundation grant number ECCS-0821565, and the Department of Energy through grant number DE-FG02-07ER46422.

References

[1] Jacobs H O, Knapp H F and Stemmer A 1999 *Rev. Sci. Instrum.* **70** 1756

[2] Oliver R A 2008 *Rep. Prog. Phys.* **71** 076501

[3] Benstetter G, Biberger R and Liu D 2009 *Thin Solid Films* **517** 5100

[4] Kalinin S V, Shao R and Bonnell D A 2005 *J. Am. Ceram. Soc.* **88** 1077

[5] Jaramillo R and Ramanathan S 2011 *Sol. Energy Mater. Sol. Cells* **95** 602

[6] Hoppe H, Glatzel T, Niggemann M, Hinsch A, Lux-Steiner M C and Sariciftci N S 2005 *Nano Lett.* **5** 269

[7] Sinensky A K and Belcher A M 2007 *Nat. Nanotechnol.* **2** 653

[8] Leung C, Maradan D, Kramer A, Howorka S, Mesquida P and Hoogenboom B W 2010 *Appl. Phys. Lett.* **97** 203703

[9] Belaidi S, Lebon F, Girard P, Leveque G and Pagano S 1998 *Appl. Phys. A* **66** S239

[10] Jacobs H O, Leuchtmann P, Horman O J and Stemmer A 1998 *J. Appl. Phys.* **84** 1168

[11] Okamoto K, Sugawara Y and Morita S 2002 *Appl. Surf. Sci.* **188** 381

[12] Machleidt T, Sparrer E, Kapusi D and Franke K-H 2009 *Meas. Sci. Technol.* **20** 084017

[13] Sommerhalter C, Matthes T W, Glatzel T, Jager-Waldau A and Lux-Steiner M C 1999 *Appl. Phys. Lett.* **75** 286

[14] Silveira W R, Muller E M, Ng T N, Dunlap D H and Marohn J A 2006 *High-sensitivity electric force microscopy of organic electronic materials and devices* (*Scanning Probe Microscopy: Electrical and Electromechanical Phenomena at the Nanoscale* vol III) ed S V Kalinin and A Gruverman. (New York: Springer Verlag) pp 788830

[15] Sadewasser S, Jelinek P, Fang C-K, Custance O, Yamada Y, Sugimoto Y, Abe M and Morita S 2009 *Phys. Rev. Lett.* **103** 266103

[16] Zhao M, Sharma V, Wei H, Birge R R, Stuart J A, Papdimitrakopoulos F and Huey B D 2008 *Nanotechnology* **19** 235704

[17] Sadewasser S, Villanueva G and Plaza J A 2006 *Appl. Phys. Lett.* **89** 033106

[18] Rosner B T and Weide D W v d 2002 *Rev. Sci. Instrum.* **73** 2505

[19] Noh J H, Nikiforov M, Kalinin S V, Vertegel A A and Rack P D 2010 *Nanotechnology* **21** 365302

[20] Brown K A, Berezovsky J and Westervelt R M 2011 *Appl. Phys. Lett.* **98** 183103

[21] Surplice N A and D'Arcy R J 1970 J. *Phys. E: Sci. Instrum.* **3** 477

[22] Baikie I D, Venderbosch E, Meyer J A and Estrup P J 1991 *Rev. Sci. Instrum.* **62** 1142075

[23] Nabhan W, Broniatowski A, De Rosny G and Equer B 1994 *Microsc. Microanal. Microstruct.* **5** 509

[24] Brown K A, Aguilar J A and Westervelt R M 2010 *Appl. Phys. Lett.* **96** 123109

[25] Brown K A and Westervelt R M 2011 *Nano Lett.* **11** 3197

[26] Brown K A, Yang B and Westervelt R M 2011 *Appl. Phys. Lett.* **100** 053110

[27] Stryahilev D and Nathan A *2002 J. Vac. Sci. Technol. A* **20** 1097

[28] Ziegler D and Stemmer A 2011 *Nanotechnology* **22** 075501

[29] Liscio A, Vincenzo P and Samorì 2008 *Adv. Funct. Mater.* **18** 907

[30] Zerweck U, Loppacher C, Otto T, Grafstrom S and Eng L M 2005 *Phys. Rev. B: Condens. Matter* **71** 125424

Figure Captions

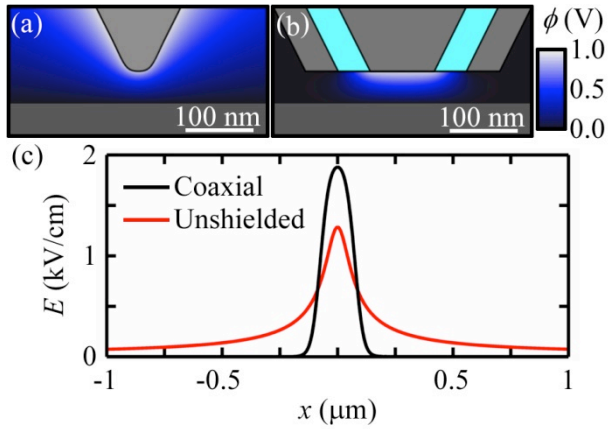

Figure 1. (a) Simulation of the electrostatic potential ϕ near the tip of an unshielded conducting probe. The probe is held at 1 V, while the substrate is grounded. The potential ϕ is seen to vary over the entire region. (b) Electrostatic simulation of the potential ϕ for a coaxial probe, showing that ϕ only varies immediately below the tip of the core conductor. The core conductor is held at 1 V while the substrate and shell electrode are grounded. (c) Electric field amplitude E at a distance 50 nm below the tip of a coaxial and an unshielded probe *vs*. distance x away from the axis of the probe. The field created by the coaxial probe is both stronger and more localized, and does not have the broad shoulders of the unshielded probe.

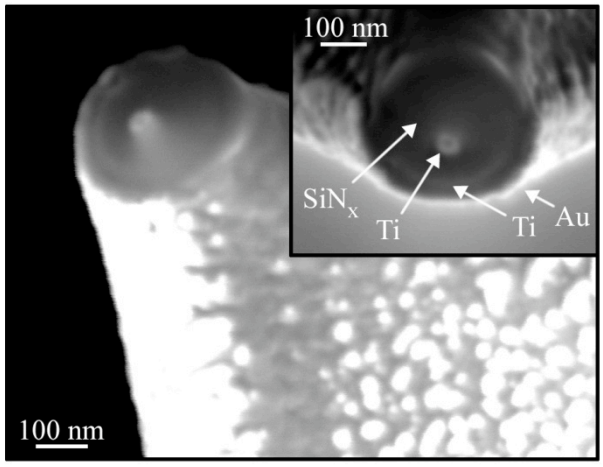

Figure 2. Scanning electron micrograph of a coaxial probe. (inset) The thin films that form the shell (Ti/Au), the insulating layer (SiN_x), and the core electrode (Ti) are visible at the tip.

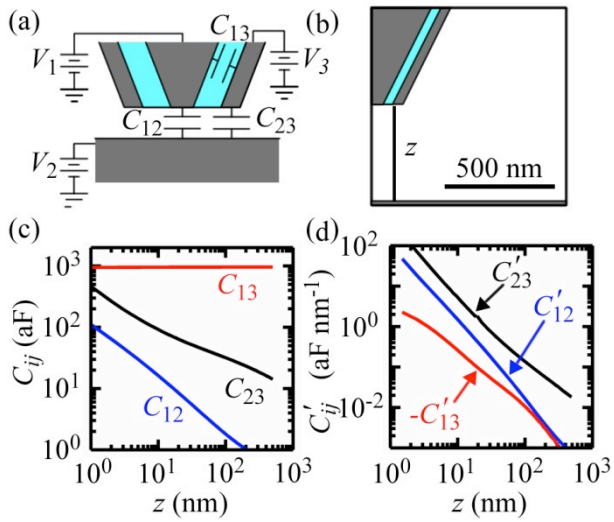

Figure 3. (a) Diagram showing the capacitances C_{ij} and applied voltages V_i of the coaxial tip-sample system. (b) Scale schematic of the region used to calculate C_{ij} using axisymmetric finite-element simulations (Maxwell 2D — Ansys Inc.). (c) Simulated capacitances C_{ij} of a coaxial tip *vs.* distance z away from a substrate. The tip-shell capacitance C_{13} is the largest. (d) The magnitude of the capacitance derivatives C'_{ij} *vs.* z calculated from the simulations in (c). The derivatives C'_{12} and C'_{23} are negative, while the derivative C'_{13} is positive.

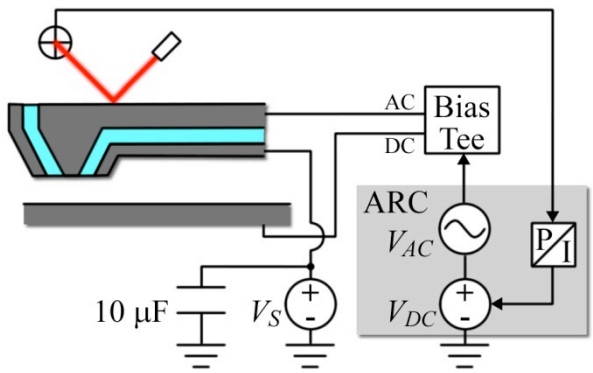

Figure 4. Schematic of the coaxial KPFM apparatus. The Asylum Research Controller (ARC) creates the AC excitation voltages V_{AC} and measures the cantilever vibrational amplitude A which controls the DC voltage V_{DC} forming a feedback loop. The voltages V_{AC} and V_{DC} are separated with a bias tee to route V_{DC} to the sample while V_{AC} is directed to the core conductor. The shell bias voltage V_S is created by an external voltage supply and tied to ground with a 10 μF capacitor to ensure V_{AC} is not present on the shell electrode.

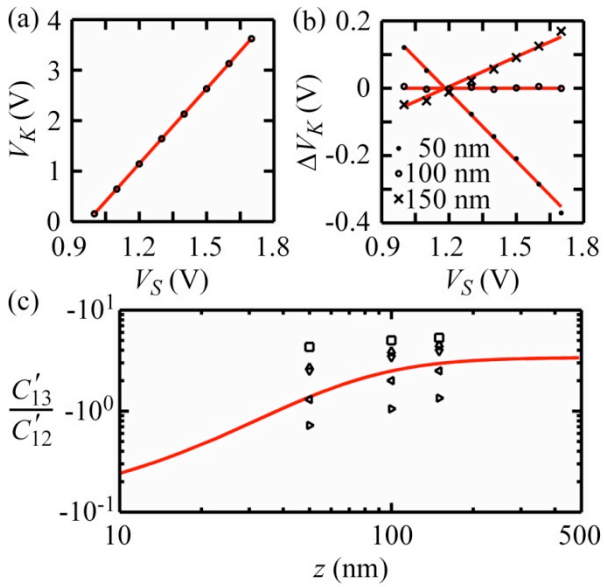

Figure 5. Procedure to calibrate a coaxial tip for Kelvin probe force microscopy to remove the effects of the shell, showing KPFM measurements of a uniform gold film by a coaxial tip at tip-sample distance z = 100 nm. (a) Measured Kelvin voltage V_K *vs.* shell bias voltage V_S; the measured points show the linear dependence on V_S predicted by equation (2). (b) Kelvin voltage ΔV_K *vs.* V_S at three different tip-sample separations z; here the difference $\Delta V_K = V_K - V_{K100}$ between V_K and the linear fit V_{K100} for z = 100 nm is shown. The coaxial probe is calibrated at the shell voltage $V_S = V_S^c$ where the three lines intersect. (c) Experimental ratios C'_{13}/C'_{12} *vs.* z for the derivatives of the core-shell and core-sample capacitances C_{13} and C_{12} for five different coaxial probes, compared with the theoretical expression for coaxial probes.

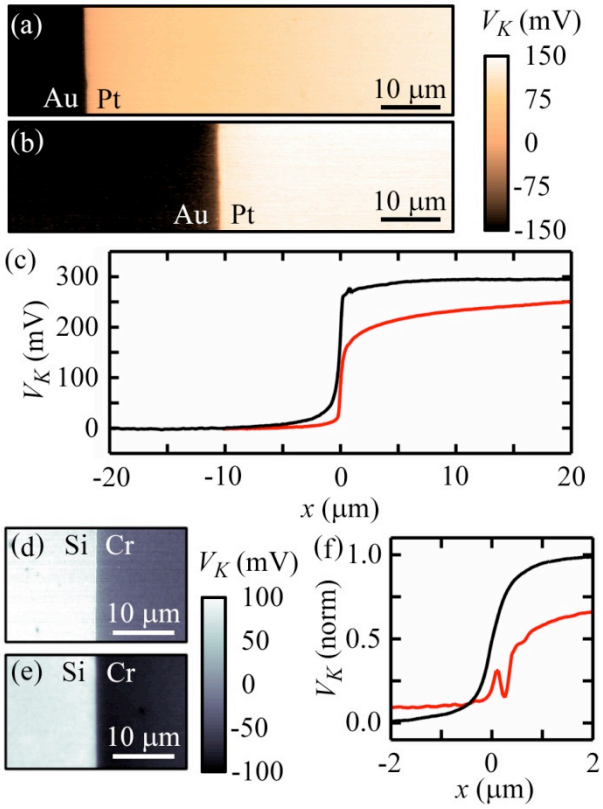

Figure 6. (a) KPFM image taken with an unshielded probe of sample with a gold region on the left and a platinum region on the right. The Kelvin voltage V_K is seen to vary over tens of microns asymmetrically due to the contribution of the cantilever. (b) KPFM image of the same sample with a coaxial probe. The Kelvin voltage V_K quickly transitions to the saturated value and the step appears symmetric. (c) Average line traces from (a) and (b) showing the step function of an unshielded probe (red line) and a coaxial probe (black line). The unshielded probe transitions very slowly after the step due to the contribution from the cantilever whereas the coaxial probe quickly saturates. (d) KPFM image taken with an unshielded probe of a sample with a heavily doped silicon region on the left and a chrome region on the right. (e) KPFM image of the same sample taken with a coaxial probe. (f) Average line traces from (d) and (e) showing the step function of an unshielded (red line) and a coaxial probe (black line). The unshielded probe exhibits topographical artifacts at the interface of the two materials whereas the coaxial probe exhibits a smooth transition.

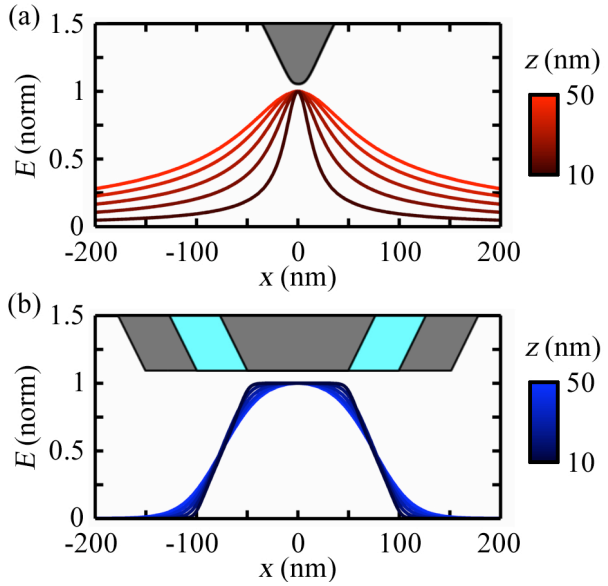

Figure 7. Axisymmetric electrostatic simulations of the electric field on a conducting substrate when an unshielded (figure 7(a)) or coaxial (figure 7(b)) probe is held at a height z above the substrate. Each panel shows a scaled schematic diagram of the probe tip used for the simulation. The unshielded probe and core conductor of the coaxial probe are held at 1 V while the substrate and shell of the coaxial probe are grounded. The electric field of each curve is normalized by its maximum value for ease of comparison.